IEEE Open Journal of
Antennas and Propagation

Received 15 November 2022; revised 16 December 2022; accepted 17 December 2022. Date of publication 4 January 2023;
date of current version 23 January 2023.

Digital Object Identifier 10.1109/OJAP.2023.3234133

Wideband MIMO Antennas for 5G Mobile Terminals

HANYANG WANG[1] (Fellow, IEEE), AND PENGFEI WU[2]

[1]Department of Wireless Technology, Huawei Technologies (UK) Ltd., RG2 6AD Reading, U.K.

[2]Department of Wireless Technology, Huawei Technologies, Ltd., Shanghai 201206, China

CORRESPONDING AUTHOR: H. WANG (e-mail: hanwanga@gmail.com)

ABSTRACT An approach of using the concept of CM (common mode) and DM (differential mode) to design two wideband antennas in a pair has been proposed. The two antennas in the antenna pair have wide bandwidth and high isolation, though they share the same radiator and total electric length of the antenna pair is just a half wavelength. A rigorous analysis has been presented to explain and illustrate the operating principle of the wideband antenna pair. An antenna design example operating in 5G New Radio (NR) N1, N2, N3, N7, N38 and N41 bands with frequency ranging from 1.71-2.69 GHz has been examined to demonstrate the effectiveness of the proposed approach. The simulated results, including S-parameters, antenna total efficiency and ECC (envelope correlation coefficient), are in good agreement with measured ones.

INDEX TERMS Handset antennas, common mode and differential mode, multiple-input multiple output (MIMO) antennas, wideband antennas, isolation.

I. INTRODUCTION

OVER the years, antenna design for mobile terminals has become increasingly difficult. This is mainly attributed to a limited space to house multiple antennas and wide frequency band requirements. The fifth generation (5G) wireless communications makes it even more challenging for mobile terminal antenna designers since it requires a large number of multiple input/multiple output (MIMO) antennas having very wide frequency bands. In these antenna designs, though antennas are placed very closely to one another, high isolation between the antennas has to be satisfied [1], [2], [3], [4]. To save antenna volume and to place more antennas in a limited space, the concepts of designing antennas in pair with high isolation have been proposed [5], [6], [7], [8], [9], [10], [11]. The concept of common mode (CM) and differential mode (DM) has been recently introduced to further reduce the antenna volume and to improve the isolation [12], [13], [14], [15], [16]. However, the main problem of the above existing work is that antennas with compact size, such as a half wavelength in electric length, usually have narrow bandwidth, since only one antenna mode or resonance is employed to cover the required very wide frequency bands. In [17], [18], [19], [20], a variety of wideband antenna pairs have been proposed to circumvent the narrow bandwidth problem, however the penalty is that the overall electric size of the antennas is much larger or the antenna configurations are very complex. Furthermore, in most of the work outlined above, the focused and examined frequency bands of 5G New Radio (NR) are N77, N78 and N79 with frequency ranging from 3.3-5.0 GHz, whereas attentions have not been given to the N1, N2, N3, N7, N38 and N41 with frequency ranging from 1.71-2.69 GHz, in which 4 x 4 MIMO antennas are also compulsory for 5G NR. The antenna with large physical size, being accommodated in a very limited space due to the lower operating frequency bands, makes antenna design even more difficult, complex and challenging.

In this paper, the CM and DM theory proposed in [12] has been significantly further developed for more compact antenna size and wider bandwidth. In comparison with the antenna in [12], the CM antenna and DM antenna in the proposed antenna pair share the same radiator, rather than using two separated antenna radiators, for the purpose of antenna size reduction, and each of the CM and DM antennas has dual resonances for impedance bandwidth improvement, instead of a single resonance. The principle on how to achieve these features using an antenna structure that supports both CM and DM has been rigorously analyzed. A realistic antenna design example has been presented and examined to demonstrate the effectiveness of the proposed

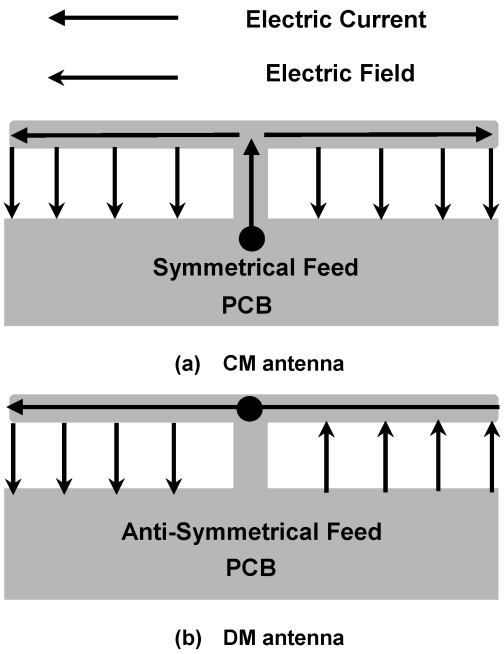

FIGURE 1. CM and DM antennas.

CM and DM approach for 5G MIMO antenna design of mobile terminals. Overall, the new contributions of this paper can be classified as: (a) the 5G NR MIMO antennas have more compact size thanks to a co-radiator being utilized to combine the CM antenna and the DM antenna; (b) The 5G NR MIMO antennas have wider bandwidth because of the innovative dual-resonance approach, and they have a half wavelength, rather than one wavelength or longer; (c) The examined frequency bands for the 5G NR MIMO antenna pair are N1, N2, N3, N7, N38 and N41 with frequency ranging from 1.71-2.69 GHz, which have seldom been studied by existing work published in the literature.

II. CM AND DM ANTENNAS

Fig. 1 shows the CM and DM antenna configuration, where the electric current and electric field distributions are illustrated, which is to some extent similar to that proposed in [12]. As can be seen, the CM antenna being fed symmetrically has symmetrical electric current and electric field distributions, while the DM antenna being fed anti-symmetrically has anti-symmetrical electric current and electric field distributions. The CM antenna can be considered as a T-shape monopole antenna having vertical polarization, whereas the DM antenna can be treated as a dipole antenna having horizontal polarization. Both the CM and DM antennas are assumed to operate at their fundamental modes though higher order modes also exist. For mobile terminals with metal frame industry design (ID), the antenna radiators could be a part of the metal frame, while for mobile terminals without metal frame the antenna radiators could be a part of PCB, stamping metal, flexible printed circuit (FPC), and laser direct structuring (LDS). The principle of achieving high isolation between the CM antenna and the

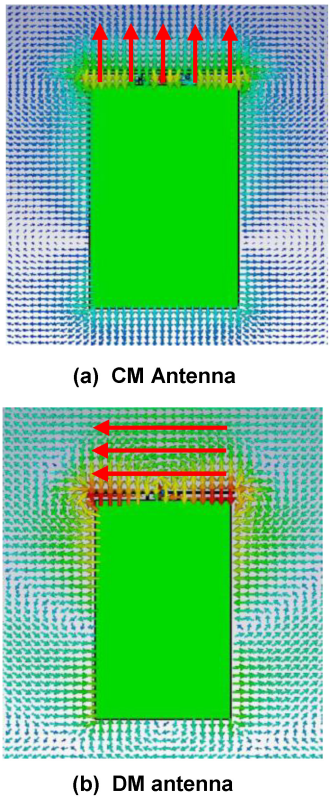

FIGURE 2. Simulated electric field distributions.

DM antenna can be explained using simulated electric field distributions of the two modes. The simulated electric field distributions of the CM antenna and the DM antenna, being fed symmetrically and anti-symmetrically respectively, are illustrated in Fig. 2. It is interesting to note that the electric field of the CM antenna indeed has vertical polarization while the electric field of the DM antenna is horizontally polarized, if the symmetrical plane of the antennas is chosen as the reference plane. Because of the polarization orthogonality of the two modes, high isolation between the two antennas is expected. Furthermore, since the configurations of the CM and DM antennas are identical, they can share the antenna radiator.

III. PRINCIPLE OF THE WIDEBAND ANTENNAS

The configuration of the proposed wideband antenna pair is shown in Figs. 3 and 4. The antenna pair comprises a printed circuit board (PCB), a radiator shared by the CM and DM antennas, connecting branches, a bridge, two feeding ports and some matching components. Port 1 is the feeding port of the CM antenna and Port 2 is the feeding port of the DM antenna. The PCB size is 130 mm x 70 mm x 1 mm. The dimensions associated with the antennas are: D = 28 mm; W = 3 mm; S = 5 mm. The values of matching components are L1 = L2 = 2.0 nH; C1 = 0.6 pf; C2 = 0.3 pf. The antennas have been simulated using CST Microwave Studio (2016 version) and the simulated S-parameters of the CM and DM antennas are depicted in Fig. 5. As can been seen, there

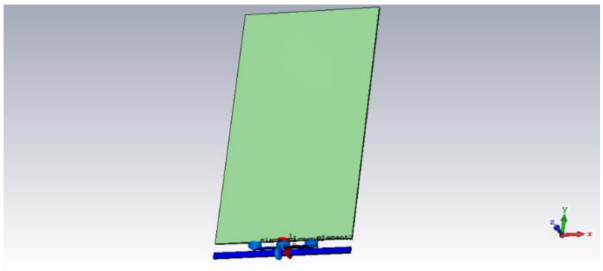

FIGURE 3. Configuration of proposed antenna pair.

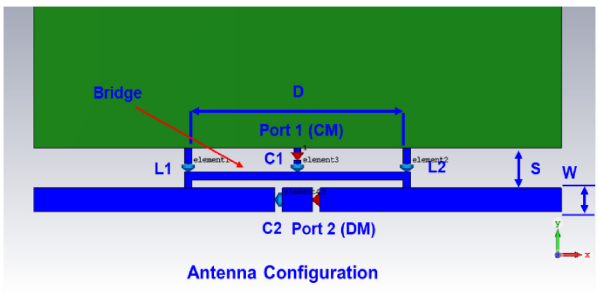

FIGURE 4. Detailed antenna configuration.

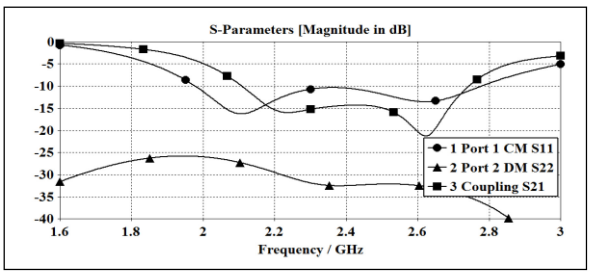

FIGURE 5. Simulated S-parameters.

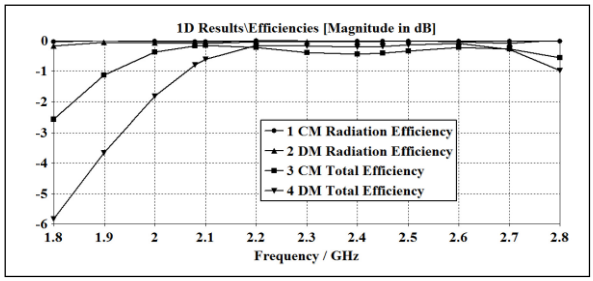

FIGURE 6. Simulated radiation and total efficiency.

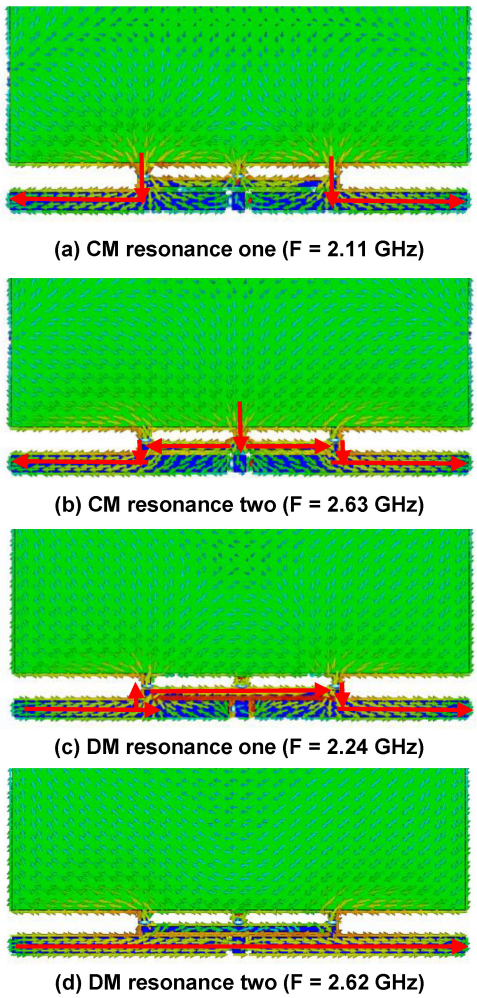

FIGURE 7. Simulated electric current distributions.

are two distinguishing resonances for both the CM antenna and the DM antenna, and good matching and isolation have been achieved for both of the antennas. The two resonant frequencies for the CM antenna are 2.11 GHz and 2.63 GHz, and the two resonant frequencies for the DM antenna are 2.24 GHz and 2.62 GHz. The radiation efficiencies and total efficiencies of the CM and DM antennas are shown in Fig. 6. As can be observed, in comparison with the CM antenna, the DM antenna's performance in terms of bandwidth and efficiency is, to some extent, worse in terms of impedance bandwidth and antenna efficiency. This is mainly because the CM antenna can effectively excite PCB modes so as to have a larger radiation aperture.

In order to comprehensively understand the operating principle of the antenna pair, it is pertinent to carry out a modal analysis based on the electric current distributions of the antennas at their resonant frequencies. Fig. 7 shows the simulated vector electric current distributions that are marked using solid red lines with arrows. For CM resonance one resonating at 2.11 GHz, two sets of symmetrically distributed electric currents, starting from the left and right sides of the PCB respectively, take the antenna tracking paths with series inductors L1 and L2 as shown in Fig. 4, and then flow to the two sides of the antenna radiator. As the series inductors can effectively increase the electric length of the antenna, its resonant frequency is relatively low. For CM resonance two resonating at 2.63 GHz, the electric current, starting from the PCB, goes through Port 1 (CM) at the centre of the PCB and the series capacitor as shown in Fig. 4, and then is divided into two symmetrically flowing paths to the left and right of the antenna radiator through the bridge as

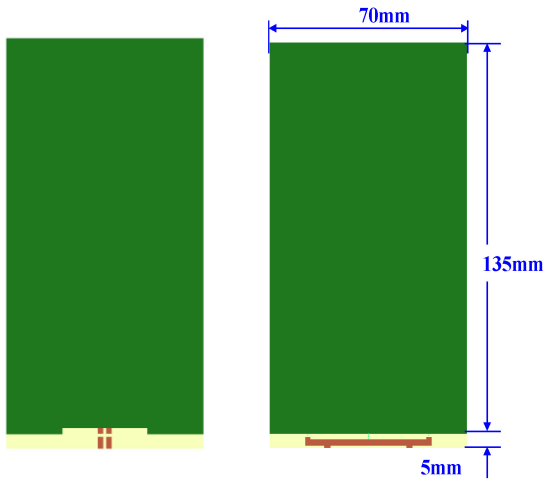

FIGURE 8. Overview of the antennas with PBC.

depicted in Fig. 4. Since the effective electric length of this CM resonance is shorter in comparison with that of CM resonance one partially due to the series capacitor, its resonant frequency is higher. For DM resonance one resonating at 2.24 GHz, the electric current starts from the left side of the antenna radiator. As the electric current is blocked by the capacitor C1 and C2 due to their low frequency filtering nature, the electric current runs over the bridge and flows to the right side of the antenna radiator. In contrast, the electric current of DM resonance two resonating at 2.62 GHz starts from the left side of the radiator and flows directly to the right side of the radiator without any blockage because of the series capacitor C2's high frequency pass nature. Since the effective electric length of this DM resonance is shorter in comparison with that of DM resonance one, its resonant frequency is higher.

IV. REALISTIC DESIGN

It should be noted that the antenna configuration shown in Fig. 4 is not a realistic one though it is a good and appropriate example to examine and explain how the CM and DM antennas operate and how the wideband feature is achieved. The unrealistic configuration is the DM feed illustrated in Fig. 4. Unlike the CM feed with symmetrical configuration, a balun is generally required to feed the DM antenna since the DM feed has an anti-symmetrical nature. Consequently, a more realistic DM antenna feed design should be utilized. The overview of the antenna design being examined is given in Fig. 8, where the CM and DM antennas are centrally placed at the bottom of the PCB. The dimensions of the PCB are 135 mm x 70 mm x 1 mm and the PCB clearance at the bottom is 5 mm. The CM feed is depicted in Fig. 9, while the DM feed is depicted in Fig. 10. The functionalities of the L/C components shown in Fig. 9 (a) are similar to those illustrated in Fig. 4. A specifically designed balun is employed to feed the DM antenna. The locations and the values of the four L/C components illustrated in Fig. 10 have to be symmetrically arranged and chosen to create the

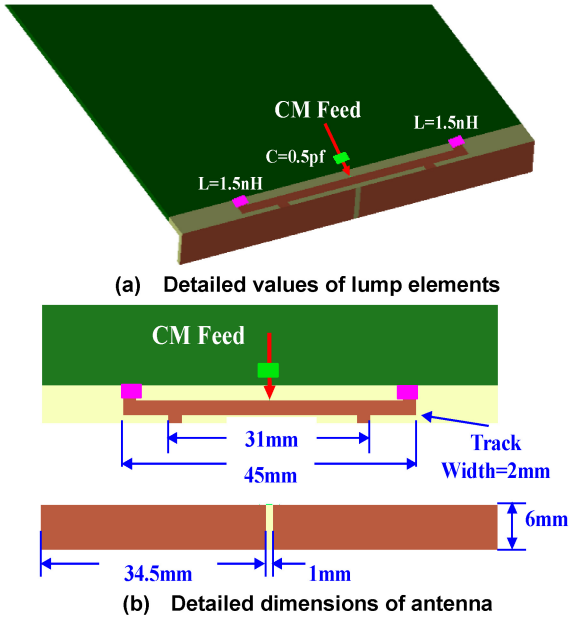

FIGURE 9. CM antenna and its feeding structure.

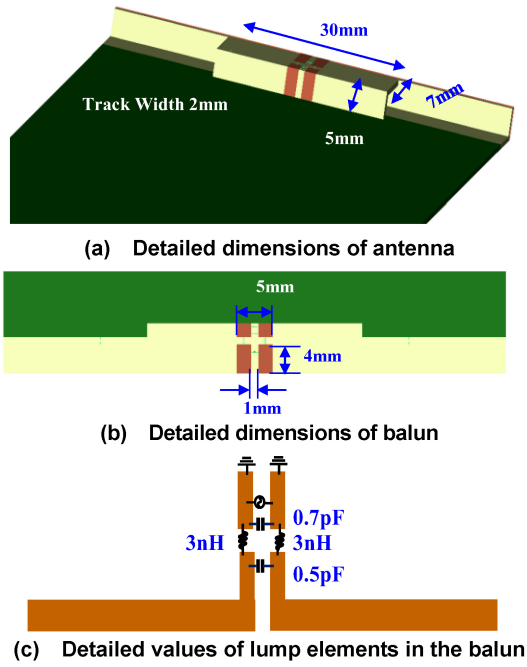

FIGURE 10. DM antenna and its feeding structure.

anti-symmetrical DM feeding structure. All the four L/C components have impacts on the resonant frequencies of the DM antenna and its isolation with the CM antenna. Similar to the CM and DM antennas shown in Fig. 4, connecting branches, a bridge and a number of matching components, including lump inductors and capacitors, are used in the antenna design. Dielectric layers with 1 mm thickness are used to support the antenna tracking, and the dielectric constant is 4.4 and the loss tangent is 0.02. The thickness of the antenna radiator is 1.0 mm. All other dimensions and values

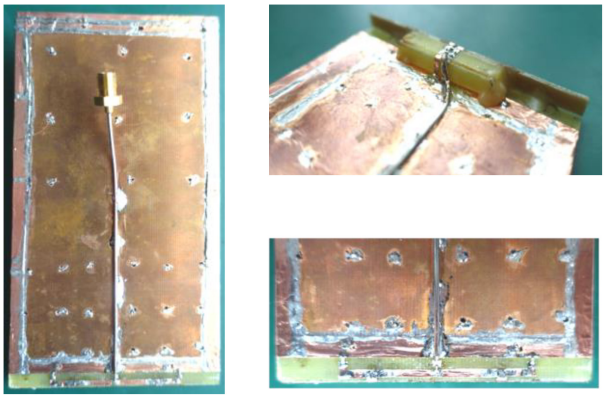

FIGURE 11. Fabricated prototyping antennas.

are also given in these figures. In comparison with antennas presented in all the references, the size of the antennas examined here is obviously larger. This is mainly because the focused frequency bands are much lower, namely NR N1, N2, N3, N7, N38 and N41 with frequency ranging from 1.71-2.69 GHz whereas the examined frequency bands in the references are typically N77, N78 and N79 with frequency ranging from 3.3-5.0 GHz. Because of the same reason, the required metal/PCB clearance in this design is also larger.

Prototyping antennas with the exactly same dimensions and values of lump elements have been fabricated to compare and validate simulated results. Fig. 11 shows photos of the prototyping antennas. In all of the following figures, the solid lines are simulated results while the dashed lines are measured results. The simulated and measured S-parameters, as a function of frequency, including the reflection coefficient of the CM port S11, the reflection coefficient of the DM port S22, and the transmission coefficient S21 representing the isolation between the two ports, are shown in Figs. 12, 13, 14, respectively. As expected, there are two distinguishing resonances for both the CM and DM antennas. The dual resonances significantly improve the impedance bandwidth of the antennas compared with the single resonance presented in [12], [13], [14], [15], [16]. For the reflection coefficient of the CM and DM, the agreements between the simulated and measured results are good, and the simulation can predict the resonant frequency points of the two modes accurately. Furthermore, it can be observed from Fig. 14 that the isolation between the CM and DM antennas is better than 26 dB. This is sufficient for most of mobile terminal antenna applications.

Figs. 15 and 16 show the simulated and measured antenna total efficiency, as a function of frequency, for the CM and DM antennas, respectively. Again, similar to the S-parameters, the simulated and the measured results are generally in good agreement. The discrepancy between the simulated and measured efficiencies for the CM antenna is mainly because the small inaccuracy in predicting resonant frequency may result in relatively large uncertainty of the reflection coefficient and efficiency. It should be emphasized here that the antenna total efficiency of the CM antenna is

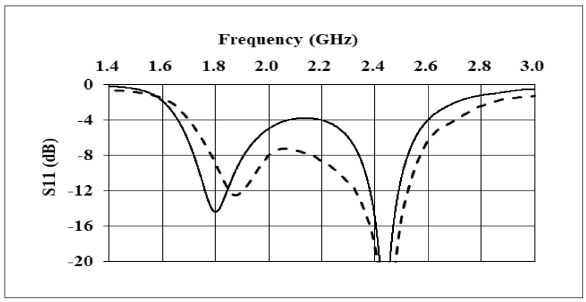

FIGURE 12. Simulated and measured S11 of CM antenna.

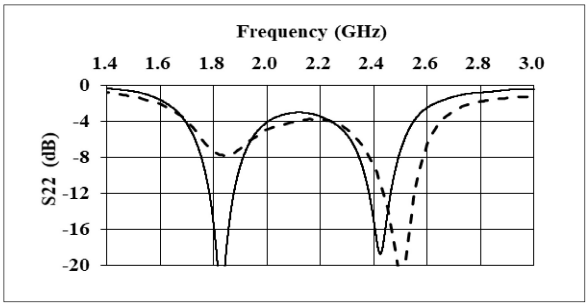

FIGURE 13. Simulated and measured S11 of DM antenna.

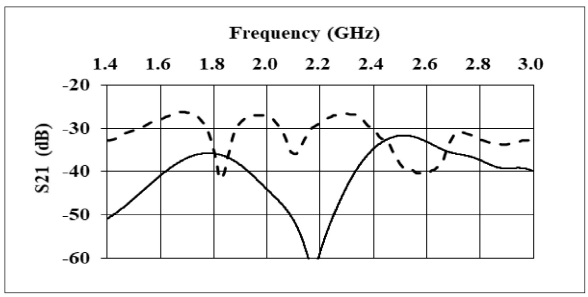

FIGURE 14. Simulated and measured S21.

better than that of the DM antenna. This is reasonable, since the DM antenna is just like a typical dipole antenna that radiates mainly through the DM antenna itself. In contrast, the CM antenna can effectively excite the connected PCB that creates additional radiation, since the PCB is a part of the CM antenna's radiator. The CM antenna has therefore much larger antenna aperture, which results in better bandwidth and total efficiency. This is a common phenomenon in mobile terminal antenna design. The penalty is that a CM antenna generally generates much more radio frequency (RF) noise than a DM antenna does because of the additional radiation from PCB or other metal parts in a mobile terminal.

Fig. 17 shows the simulated and measured envelop correlation coefficient (ECC) of the CM and DM antennas. As can be seen, though the CM and DM antennas share the same radiator and have a very compact size in this design example, both the simulated and measured ECC are smaller than 0.1 across the frequency band. The discrepancy between the simulated and measured ECC is probably thanks to the value being too small to measure very accurately. The ECC

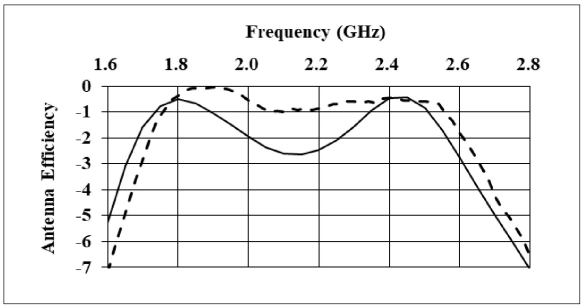

FIGURE 15. Simulated and measured CM total efficiency.

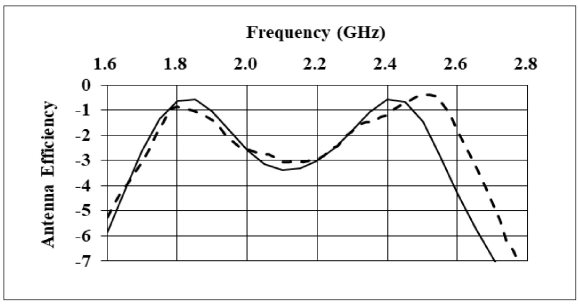

FIGURE 16. Simulated and measured DM total efficiency.

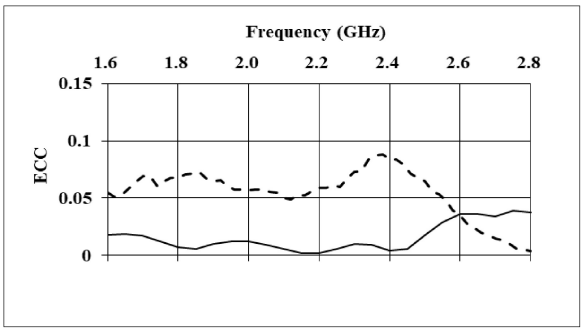

FIGURE 17. Simulated and measured ECC.

is substantially lower than that of most MIMO antennas for mobile terminals. The simulated radiation patterns of the CM and DM antennas are illustrated in Fig. 18. Since the radiation patterns at the whole frequency band are very similar, the radiation pattern at one frequency point, namely at 2.1 GHz, is presented for both the CM and DM antennas. As can be observed from Fig. 18(a), for the CM antenna the maximum radiation direction is very close to the horizontal plane if the phone is placed upright and the radiation is virtually isotropic at this plane. It is also interesting to note from Fig. 18(b) that the maximum radiation direction of the DM antenna is at the top direction and the radiation at the horizontal plane is much weaker. This indicates that the two antenna radiation patterns are complementary. In addition to the polarization orthogonality of CM and DM, this feature could be also used to explain why the high isolation and low ECC between the CM and DM antennas have been achieved. It should be noted here that most mobile

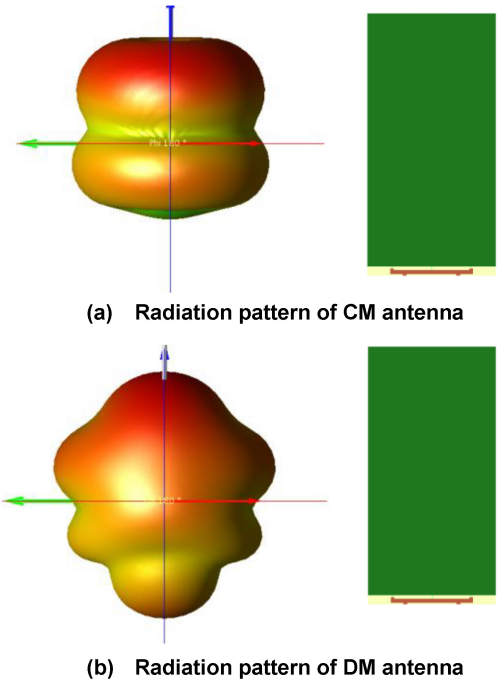

FIGURE 18. Simulated radiation pattern at 2.1 GHz.

operators require the specification of total radiated power (TRP) and total isotropic sensitivity (TIS) that are directly related to antenna efficiency. This is because the orientation of a handheld device could be arbitrary, and omnidirectional radiation pattern is usually preferred. Consequently, antenna gain is usually not an important parameter in mobile terminal antenna design, and it therefore has not been presented here.

V. CONCLUSION

A wideband MIMO antenna pair for 5G Sub 6GHz has been proposed and analysed for the applications of mobile terminals using the concept of CM and DM antennas. The MIMO antenna pair has very compact size because the two antennas share the same antenna radiator. An innovative and rigorous approach utilizing a bridge, branches and lump elements, including inductors and capacitors, has been proposed and developed to create additional resonances for both the CM and DM antennas in the antenna pair without increasing the size of the antenna radiator. The operating principle of the wideband approach has been comprehensively and rigorously explained using the simulated modal current distributions and the concept of frequency filtering properties of the lump elements. The main advantages of the proposed CM and DM antenna pair can be summarized as: very compact, wide bandwidth, complementary and orthogonally polarized radiation patterns, high isolation and low ECC. To the authors' knowledge, the proposed CM and DM antenna pair currently represents one of the best MIMO antenna solutions for mobile terminals. The proposed CM and DM antenna pair with dual resonances is expected to have significant impacts on the 5G MIMO antenna design of mobile terminals and many other areas in mobile communications.

REFERENCES

[1] I. R. Barani and K.-L. Wong, "Integrated inverted-F and open-slot antennas in the metal-framed smartphone for 2×2 LTE LB and 4×4 LTE M/HB MIMO operations," *IEEE Trans. Antennas Propag.*, vol. 66, no. 10, pp. 5004–5012, Oct. 2018.

[2] H. Xu, H. Zhou, S. Gao, H. Y. Wang, and Y. J. Cheng, "Multimode decoupling technique with independent tuning characteristic for mobile terminals," *IEEE Trans. Antennas Propag.*, vol. 65, no. 12, pp. 6739–6751, Dec. 2017.

[3] A. Ren, Y. Liu, and C.-Y.-D. Sim, "A compact building block with two shared-aperture antennas for eight-antenna MIMO array in metal-rimmed smartphone," *IEEE Trans. Antennas Propag.*, vol. 67, no. 10, pp. 6430–6438, Oct. 2019.

[4] Y. X. Li, C.-Y.-D. Sim, Y. Luo, and G. L. Yang, "High-isolation 3.5 GHz eight-antenna MIMO array using balanced open-slot antenna element for 5G smartphones," *IEEE Trans. Antennas Propag.*, vol. 67, no. 6, pp. 3820–3830, Jun. 2019.

[5] K.-L. Wong, C.-Y. Tsai, and J.-Y. Lu, "Two asymmetrically mirrored gap-coupled loop antennas as a compact building block for eight-antenna MIMO array in the future smartphone," *IEEE Trans. Antennas Propag.*, vol. 65, no. 4, pp. 1765–1778, Apr. 2017.

[6] J. Sui and K.-L. Wu, "Self-curing decoupling technique for two inverted-F antennas with capacitive loads," *IEEE Trans. Antennas Propag.*, vol. 66, no. 3, pp. 1093–1101, Mar. 2018.

[7] L. B. Sun, Z. H. Feng, Y. Li, and Z. J. Zhang, "Tightly arranged orthogonal mode antenna for 5G MIMO mobile terminal," *Microw. Opt. Technol. Lett.*, vol. 60, no. 7, pp. 1751–1756, Jul. 2018.

[8] L. B. Sun, H. Feng, Y. Li, and Z. Zhang, "Compact 5G MIMO mobile phone antennas with tightly arranged orthogonal-mode pairs," *IEEE Trans. Antennas Propag.*, vol. 66, no. 11, pp. 6364–6369, Nov. 2018.

[9] Z. Y. Ren, A. P. Zhao, and S. J. Wu, "MIMO antenna with compact decoupled antenna pairs for 5G mobile terminals," *IEEE Antennas Wireless Propag. Lett.*, vol. 18, pp. 1367–1371, 2019.

[10] C. J. Deng, D. Liu, and X. Lv, "Tightly arranged four-element MIMO antennas for 5G mobile terminals," *IEEE Trans. Antennas Propag.*, vol. 67, no. 10, pp. 6353–6361, Oct. 2019.

[11] J. W. Sui, Y. H. Dou, X. D. Mei, and K.-L. Wu, "Self-curing decoupling technique for MIMO antenna arrays in mobile terminals," *IEEE Trans. Antennas Propag.*, vol. 68, no. 2, pp. 838–849, Feb. 2020.

[12] H. Xu, S. S. Gao, H. Zhou, H. Y. Wang, and Y. J. Cheng, "A highly integrated MIMO antenna unit: Differential/common mode design," *IEEE Trans. Antennas Propag.*, vol. 67, no. 11, pp. 6724–6734, Nov. 2019.

[13] L. Chang, Y. F. Yu, K. P. Wei, and H. Y. Wang, "Polarization-orthogonal co-frequency dual antenna pair suitable for 5G MIMO smartphone with metallic bezels," *IEEE Trans. Antennas Propag.*, vol. 67, no. 8, pp. 5212–5220, Aug. 2019.

[14] L. Chang, Y. F. Yu, K. P. Wei, and H. Y. Wang, "Orthogonally polarized dual antenna pair with high isolation and balanced high performance for 5G MIMO smartphone," *IEEE Trans. Antennas Propag.*, vol. 68, no. 5, pp. 3487–3495, May 2020.

[15] L. B. Sun, Y. Li, Z. J. Zhang, and H. Y. Wang, "Self-decoupled MIMO antenna pair with shared radiator for 5G smartphones," *IEEE Trans. Antennas Propag.*, vol. 68, no. 5, pp. 3423–3432, May 2020.

[16] Y. Ye, X. Zhao, and J. Y. Wang, "Compact high-isolated MIMO antenna module with chip capacitive decoupler for 5G mobile terminals," *IEEE Antennas Wireless Propag. Lett.*, vol. 21, pp. 928–932, 2022.

[17] L. Chang, G. L. Zhang, and H. Y. Wang, "Dual-band antenna pair with lumped filters for 5G MIMO terminals," *IEEE Trans. Antennas Propag.*, vol. 69, no. 9, pp. 5413–5423, Sep. 2021.

[18] K.-L. Wong, B.-W. Lin, and W.-Y. Li, "Dual-band dual inverted-F/loop antennas as a compact decoupled building block for forming eight 3.5/5.8-GHz MIMO antennas in the future smartphone," *Microw. Opt. Technol. Lett.*, vol. 59, no. 11, pp. 2715–2721, Nov. 2017.

[19] K.-L. Wong, Y.-H. Chen, and W.-Y. Li, "Decoupled compact ultra-wideband MIMO antennas covering 3300 6000 MHz for the fifth-generation mobile and 5GHz-WLAN operations in the future smartphone," *Microw. Opt. Technol. Lett.*, vol. 60, no. 10, pp. 2345–2351, Oct. 2018.

[20] L. B. Sun, Y. Li, Z. J. Zhang, and Z. H. Feng, "Wideband 5G MIMO antenna with integrated orthogonal-mode dual-antenna pairs for metal-rimmed smartphones," *IEEE Trans. Antennas Propag.*, vol. 68, no. 4, pp. 2494–2503, Apr. 2020.